Computer modelling of defect structure and rare earth doping in $LiCaAlF_6$ and $LiSrAlF_6$

2003 J. Phys.: Condens. Matter 15 2523

(http://iopscience.iop.org/0953-8984/15/17/308)

INSTITUTE OF PHYSICS PUBLISHING JOURNAL OF PHYSICS: CONDENSED MATTER

J. Phys.: Condens. Matter **15** (2003) 2523–2533 PII: S0953-8984(03)53195-2

Computer modelling of defect structure and rare earth doping in $LiCaAlF_6$ and $LiSrAlF_6$

J B Amaral[1], D F Plant[2], M E G Valerio[1] and R A Jackson[2,3]

[1] Departamento de Física, Universidade Federal de Sergipe, 49 100-000 São Cristovão-SE, Brazil
[2] Lennard-Jones Laboratories, School of Chemistry and Physics, Keele University, Keele, Staffordshire ST5 5BG, UK

E-mail: mvalerio@fisica.ufs.br and r.a.jackson@chem.keele.ac.uk

Received 9 September 2002, in final form 14 March 2003
Published 22 April 2003
Online at stacks.iop.org/JPhysCM/15/2523

Abstract

This paper describes a computational study of the mixed metal fluorides $LiCaAlF_6$ and $LiSrAlF_6$, which have potential technological applications when doped with a range of elements, especially those from the rare earth series. Potentials are derived to represent the structure and properties of the undoped materials, then defect properties are calculated, and finally solution energies for rare earth elements are calculated, enabling preferred dopant sites and charge compensation mechanisms to be predicted.

1. Introduction

The mixed metal fluorides $LiCaAlF_6$ and $LiSrAlF_6$ are being investigated for use in photonic devices because they are good hosts for optically active cations and can be grown easily [1]. Recent examples of applications include the use of Nd^{3+}–$LiCaAlF_6$ in photolithography [2] and Ce^{3+}–$LiCaAlF_6$ in UV chirped-pulse amplification [3]. In addition, both Ce^{3+}-doped $LiCaAlF_6$ and $LiSrAlF_6$ have been reported as leading candidates for tuneable solid-state lasers in the UV region [4, 5]. Computer modelling is a useful technique for determination of the defect properties of materials and the location of dopant ions, as shown in a recent application to $BaLiF_3$ [6]. The technique is based on description of interactions between ions by effective potentials, structural determination by lattice energy minimization, and use of the Mott–Littleton method [7] to model defects and dopants. In the present paper a potential is fitted to the structure of $LiCaAlF_6$ and $LiSrAlF_6$, which is then used to calculate their defect properties—principally energies of formation of defects, which lead to predictions of the form of defect disorder to be expected. Then, using a consistently derived set of potentials for rare earth ions in fluorides [8], defect formation energies and solution energies are calculated for rare earth ions at all possible dopant sites in $LiCaAlF_6$ and $LiSrAlF_6$, noting that there are three possible dopant sites and a wide range of possible charge compensation schemes.

[3] Author to whom any correspondence should be addressed.

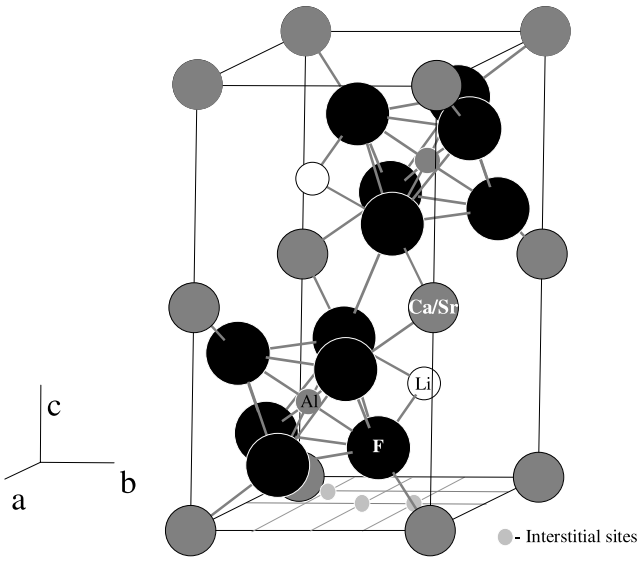

Figure 1. Unit cell representation of the $LiCaAlF_6$/$LiCaAlF_6$. The grey circles indicate the positions of the three interstitial sites.

Table 1. Experimental and calculated lattice parameters for (i) $LiCaAlF_6$, (ii) $LiSrAlF_6$.

Parameter	Exp.	Calc.	Diff. (%)
	(i) $LiCaAlF_6$ [9]		
$a = b$ (Å)	5.01	5.03	0.42
c (Å)	9.64	9.62	−0.24
γ (deg)	120.00	120.00	0.00
	(ii) $LiSrAlF_6$ [10]		
$a = b$ (Å)	5.07	5.15	−1.57
c (Å)	10.19	10.56	−3.63
γ (deg)	120.00	120.00	0.00

2. Structural information

$LiCaAlF_6$ and $LiSrAlF_6$ both crystallize in the hexagonal crystal system with space group $P\bar{3}1c$ [9, 10]. The lattice parameters are given in table 1. The unit cell is illustrated in figure 1.

3. Computational method

The methodology adopted in this paper has been described extensively in previous papers [11, 12] and follows the procedure adopted for rare earth ions in $BaLiF_3$ described in [6]. A brief summary of the important points of procedure now follows.

3.1. Derivation of potentials

Interatomic potentials were taken from literature sources with appropriate refitting where required. The Li–F and F–F parameters are from a compilation by Binks [13], while the Ca–F, Sr–F and Al–F parameters were fitted to the structure of $LiCaAlF_6$ and $LiSrAlF_6$. Table 2 lists

Table 2. Interatomic potentials for $LiCaAlF_6$ and $LiSrAlF_6$.

Interaction	A (eV)	ρ (Å)	C (eV Å^6)	k (eV Å^{-2})
Li core F shell	443.83	0.2714	0.0	—
Al core F shell	1400.00	0.2571	0.0	—
Ca core F shell	3400.00	0.2661	0.0	—
Sr core F shell	3400.00	0.2906	0.0	—
F shell F shell	911.69	0.2707	13.80	—
F core F shell	—	—	—	24.36

the potential parameters, and table 1 shows the comparison of calculated and experimental lattice parameters. It is noted that agreement of 0.5 and 4% or better is obtained for $LiCaAlF_6$ and $LiSrAlF_6$ respectively, giving confidence in using the potential to calculate properties not included in the fitting procedure.

3.2. Defect calculations

Calculations of defects and of rare earth doping were performed using the Mott–Littleton method [7] in which atoms in a spherical region immediately surrounding the defect are treated explicitly, and a continuum approach is used for more distant regions of the lattice. This method has been widely and successfully used in modelling defects in ionic solids; a related application to $BaLiF_3$ is given in [6, 11, 12].

In calculating the energetics of doping by rare earth ions, the defect formation energy is first calculated. This quantity cannot be used for comparison purposes, and instead the solution energy is calculated, which is defined as the total energy involved in the doping process, including charge compensation if needed. The calculation of solution energies, and the different reaction schemes involved in rare earth doping, are given in section 4.2.

4. Results

4.1. Defect formation in $LiCaAlF_6$ and $LiSrAlF_6$

Energies of formation of the important defects in $LiCaAlF_6$ and $LiSrAlF_6$ have been calculated, considering three interstitial sites, at $(\frac{1}{4}, \frac{1}{4}, 0)$, $(\frac{1}{2}, \frac{1}{2}, 0)$ and $(\frac{3}{4}, \frac{1}{2}, 0)$.

The energies have been combined to form Frenkel, Schottky and pseudo Schottky (LiF, CaF_2/SrF_2 and AlF_3) energies, and in addition, anti-Schottky and pseudo anti-Schottky energies. The latter correspond to the formation of an appropriate formula unit of interstitial defects, and have been discussed by Chadwick for the example of alkali halide systems [14]. Their formation process is explained in the following reactions for $LiCaAlF_6$:

$$\begin{aligned} LiCaAlF_6 &\rightarrow Li_i^{\bullet} + Ca_i^{\bullet\bullet} + Al_i^{\bullet\bullet\bullet} + 6F_i' \\ LiF &\rightarrow Li_i^{\bullet} + F_i' \\ CaF_2 &\rightarrow Ca_i^{\bullet\bullet} + 2F_i' \\ AlF_3 &\rightarrow Al_i^{\bullet\bullet\bullet} + 3F_i' \end{aligned}$$

Similar reactions apply to $LiSrAlF_6$.

The energies are reported in table 3, noting that for the anti-Schottky and pseudo anti-Schottky energies, only the configurations with lowest energies are reported. Table 4 gives the lattice energies required in the calculation of solution energies; these are calculated values taken from a previous study by the authors [8].

Table 3. Formation energies of defects in $LiCaAlF_6$ and $LiSrAlF_6$. nc denotes non-convergence.

		Energies (eV)	
		$LiCaAlF_6$	$LiSrAlF_6$
Basic defects			
V'_{Li}		8.32	8.52
V''_{Ca}/V''_{Sr}		23.20	20.94
V'''_{Al}		60.93	59.00
$V^{\bullet}_{F}$		6.39	5.96
$Li^{\bullet}_{i}$	$(\frac{1}{4}\ \frac{1}{4}\ 0)$	−5.03	−5.82
	$(\frac{1}{2}\ \frac{1}{2}\ 0)$	−5.03	−5.25
	$(\frac{3}{4}\ \frac{1}{2}\ 0)$	−5.87	−5.82
$Ca^{\bullet\bullet}_{i}/Sr^{\bullet\bullet}_{i}$	$(\frac{1}{4}\ \frac{1}{4}\ 0)$	nc	−12.23
	$(\frac{1}{2}\ \frac{1}{2}\ 0)$	−12.74	−10.69
	$(\frac{3}{4}\ \frac{1}{2}\ 0)$	−14.86	−16.26
$Al^{\bullet\bullet\bullet}_{i}$	$(\frac{1}{4}\ \frac{1}{4}\ 0)$	−44.09	−45.50
	$(\frac{1}{2}\ \frac{1}{2}\ 0)$	−43.29	−44.48
	$(\frac{3}{4}\ \frac{1}{2}\ 0)$	−45.26	−45.51
F'_{i}	$(\frac{1}{4}\ \frac{1}{4}\ 0)$	−2.38	−2.36
	$(\frac{1}{2}\ \frac{1}{2}\ 0)$	−2.02	−1.92
	$(\frac{3}{4}\ \frac{1}{2}\ 0)$	−2.02	−2.46
Frenkel and Schottky defects			
Anionic Frenkel	$(\frac{1}{4}\ \frac{1}{4}\ 0)$	4.01	3.60
	$(\frac{1}{2}\ \frac{1}{2}\ 0)$	4.37	4.04
	$(\frac{3}{4}\ \frac{1}{2}\ 0)$	4.37	3.50
Cationic Frenkel			
Li	$(\frac{1}{4}\ \frac{1}{4}\ 0)$	3.29	2.70
	$(\frac{1}{2}\ \frac{1}{2}\ 0)$	3.29	3.27
	$(\frac{3}{4}\ \frac{1}{2}\ 0)$	2.45	2.70
Ca/Sr	$(\frac{1}{4}\ \frac{1}{4}\ 0)$	nc	8.71
	$(\frac{1}{2}\ \frac{1}{2}\ 0)$	10.46	10.25
	$(\frac{3}{4}\ \frac{1}{2}\ 0)$	8.34	4.68
Al	$(\frac{1}{4}\ \frac{1}{4}\ 0)$	16.84	13.50
	$(\frac{1}{2}\ \frac{1}{2}\ 0)$	17.64	14.52
	$(\frac{3}{4}\ \frac{1}{2}\ 0)$	15.67	13.49
Schottky		28.45	24.13
Pseudo Schottky	LiF	3.78	3.55
	CaF_2/SrF_2	8.99	8.39
	AlF_3	16.11	12.89
Anti-Schottky		22.07	17.74
Pseudo anti-Schottky	LiF	2.68	2.65
	CaF_2/SrF_2	7.37	3.29
	AlF_3	11.59	11.35

Table 4. Lattice energies (calculated, [8]).

	Lattice energies (eV)
$LiCaAlF_6$	−102.34
$LiSrAlF_6$	−100.09
LiF	−10.93
CaF_2	−26.99
SrF_2	−24.47
AlF_3	−63.99
LaF_3	−49.70
CeF_3	−50.15
PrF_3	−50.60
NdF_3	−51.04
SmF_3	−51.24
EuF_3	−52.4
GdF_3	−52.24
TbF_3	−52.23
DyF_3	−52.85
HoF_3	−53.37
ErF_3	−53.47
TmF_3	−53.63
YbF_3	−53.96
LuF_3	−54.25

4.2. Rare earth doping in $LiCaAlF_6$ and $LiSrAlF_6$

As has already been noted, in addition to defect formation energies for substitution of rare earth ions at cation sites it is necessary to calculate solution energies, which include all energy terms involved in the solution process. When rare earth ions substitute at the Al^{3+} site, no charge compensation is needed, but substitution at Ca^{2+}/Sr^{2+} sites or Li^+ sites requires the formation of cation vacancies or F^- interstitials. In all cases the rare earth ion must be formed by dissociation of REF_3, and any displaced cations and F^- ions accounted for. The following solution energy schemes have been considered:

(i) M^{3+} at Al^{3+} (no charge compensation).
(ii) M^{3+} at Ca^{2+}/Sr^{2+}, with charge compensation by Ca^{2+}/Sr^{2+} vacancies.
(iii) M^{3+} at Ca^{2+}/Sr^{2+}, with charge compensation by Li^+ vacancies.
(iv) M^{3+} at Ca^{2+}/Sr^{2+}, with charge compensation by F^- interstitials (three interstitial sites considered).
(v) M^{3+} at Li^+, with charge compensation by Li^+ vacancies.
(vi) M^{3+} at Li^+, with charge compensation by Ca^{2+}/Sr^{2+} vacancies.
(vii) M^{3+} at Li^+, with charge compensation by F^- interstitials (three interstitial sites considered).

Table 5 gives reactions for the above schemes for $LiCaAlF_6$; corresponding reactions for $LiSrAlF_6$ are obtained by substituting Sr for Ca.

Energies for substitution of rare earth ions at Al^{3+}, Ca^{2+}/Sr^{2+} and Li^+ sites are given in table 6.

Solution energies have been reported in two ways. Tables 7(a) and (b) give the solution energies for schemes (i)–(iv) above, assuming that there is no binding energy between the M^{3+} ion and the charge compensating defect, where present. Tables 8(a) and (b) give the corresponding solution energies including this defect–defect interaction term. Tables 9(a) and (b) give the unbound solution energies for schemes (v)–(vii) (solution at the Li^+ site);

Table 5. Reaction schemes for solution of rare earth dopants in $LiCaAlF_6$ (see section 4.2 for details); similar schemes apply to $LiSrAlF_6$.

(i)	$MF_3 + Al_{Al} \rightarrow M_{Al} + AlF_3$
(ii)	$MF_3 + Ca_{Ca} \rightarrow M^{\bullet}_{Ca} + \frac{1}{2}V''_{Ca} + \frac{3}{2}CaF_2$
(iii)	$MF_3 + Ca_{Ca} \rightarrow M^{\bullet}_{Ca} + V'_{Li} + LiF + CaF_2$
(iv)	$MF_3 + Ca_{Ca} \rightarrow M^{\bullet}_{Ca} + F_i{}' + CaF_2$ (three interstitial sites considered)
(v)	$MF_3 + Li_{Li} \rightarrow M^{\bullet\bullet}_{Li} + 2V'_{Li} + 3LiF$
(vi)	$MF_3 + Li_{Li} \rightarrow M^{\bullet\bullet}_{Li} + V''_{Ca} + LiF + CaF_2$
(vii)	$MF_3 + Li_{Li} \rightarrow M^{\bullet\bullet}_{Li} + 2F_i{}' + LiF$ (three interstitial sites considered)

Table 6. Energies for the substitution of rare earth dopant ions on to lattice sites.

	$LiCaAlF_6$			$LiSrAlF_6$		
Host	M_{Al}	$M^{\bullet}_{Ca}$	$M^{\bullet\bullet}_{Li}$	M_{Al}	$M^{\bullet}_{Sr}$	$M^{\bullet\bullet}_{Li}$
La	18.49	−17.39	−23.68	18.15	−19.77	−24.54
Ce	17.80	−17.85	−24.32	19.90	−20.18	−25.18
Pr	17.12	−18.30	−24.96	16.81	−20.59	−25.81
Nd	16.51	−18.74	−25.55	16.22	−20.98	−26.37
Sm	15.75	−19.09	−26.20	15.49	−21.30	−27.02
Eu	14.70	−19.92	−27.23	14.46	−22.07	−28.03
Gd	14.48	−19.96	−27.40	14.25	−22.10	−28.20
Tb	14.30	−20.04	−27.55	14.08	−22.17	−28.35
Dy	13.58	−20.52	−28.23	13.38	−22.64	−29.02
Ho	13.29	−21.01	−28.61	13.07	−23.09	−29.38
Er	12.84	−21.16	−28.97	12.65	−23.23	−29.74
Tm	12.46	−21.27	−29.27	12.28	−23.32	−30.04
Yb	12.40	−21.58	−29.43	12.21	−23.63	−30.19
Lu	11.75	−21.79	−29.95	11.59	−23.81	−30.71

table 10 gives the corresponding bound solution energies for scheme (vi) (substitution at the Li^+ site with charge compensation by formation of Ca^{2+}/Sr^{2+} vacancies).

5. Discussion of results

5.1. Defect formation

From table 3 it can be seen that the Li^+ Frenkel formation and LiF pseudo anti-Schottky defects are the most likely form of defect disorder in both $LiCaAlF_6$ and $LiSrAlF_6$. Since the difference in formation energies between the two defects is small for both systems (∼9% for $LiCaAlF_6$ and ∼2% for $LiSrAlF_6$), it is expected that these two types will dominate all defect-driven processes in the pure systems as temperature increases. Considering this further, for $LiCaAlF_6$ the Li^+ Frenkel defect has the lowest formation energy, while for $LiSrAlF_6$ the LiF pseudo anti-Schottky defect has the lowest formation energy. This result can be understood in terms of the space available for interstitial ions in the two host crystals. The lattice parameters of $LiCaAlF_6$ are smaller than those of $LiSrAlF_6$, implying that the interstitial sites have smaller volumes. Li^+ can be easily fitted in the interstitial sites in both hosts, since its ionic radius is quite small, and a significant difference between the formation energies of Li^+ interstitials in $LiCaAlF_6$ and $LiSrAlF_6$ is not expected. The values shown in table 3 indicate that this difference is about 1%. However, F^- is a large ion, and it is expected that the lattice distortion,

Table 7. Solution energies (in eV) for rare earth dopants (M) in (a) $LiCaAlF_6$ at Al^{3+} and Ca^{2+} sites (b) $LiSrAlF_6$ at Al^{3+} and Sr^{2+} sites (schemes (i)–(iv) in table 5) assuming the defects to be unbound. Lowest energies are highlighted in bold.

(a)	Scheme from table 5	M_{Al} (i)	$M^{\bullet}_{Ca}-\frac{1}{2}V''_{Ca}$ (ii)	$M^{\bullet}_{Ca}-V'_{Li}$ (iii)	$M^{\bullet}_{Ca}-F_i'$ (iv) F_i' at $(\frac{1}{4}\ \frac{1}{4}\ 0)$	$M^{\bullet}_{Ca}-F_i'$ (iv) F_i' at $(\frac{1}{2}\ \frac{1}{2}\ 0)$	$M^{\bullet}_{Ca}-F_i'$ (iv) F_i' at $(\frac{3}{4}\ \frac{1}{2}\ 0)$
	La	4.20	3.43	**2.71**	2.94	3.30	3.30
	Ce	3.96	3.48	**2.70**	2.93	3.29	3.29
	Pr	3.72	3.48	**2.70**	2.93	3.29	3.29
	Nd	3.56	3.48	**2.70**	2.93	3.29	3.29
	Sm	3.00	3.33	**2.55**	2.78	3.14	3.14
	Eu	2.95	3.50	**2.72**	2.95	3.31	3.31
	Gd	2.72	3.46	**2.68**	2.91	3.27	3.27
	Tb	**2.54**	3.37	2.59	2.82	3.18	3.18
	Dy	**2.44**	3.52	2.73	2.96	3.15	3.15
	Ho	**2.67**	3.54	2.76	2.99	3.18	3.18
	Er	**2.32**	3.49	2.71	2.94	3.30	3.30
	Tm	**2.10**	3.54	2.76	2.99	3.18	3.18
	Yb	**2.37**	3.56	2.78	3.01	3.20	3.20
	Lu	**2.01**	3.64	2.86	3.09	3.45	3.45
(b)	Scheme from table 5	M_{Al} (i)	$M^{\bullet}_{Sr}-\frac{1}{2}V''_{Sr}$ (ii)	$M^{\bullet}_{Sr}-V'_{Li}$ (iii)	$M^{\bullet}_{Sr}-F_i'$ (iv) F_i' at $(\frac{1}{4}\ \frac{1}{4}\ 0)$	$M^{\bullet}_{Sr}-F_i'$ (iv) F_i' at $(\frac{1}{2}\ \frac{1}{2}\ 0)$	$M^{\bullet}_{Sr}-F_i'$ (iv) F_i' at $(\frac{3}{4}\ \frac{1}{2}\ 0)$
	La	3.86	3.70	3.05	3.10	3.54	**3.00**
	Ce	6.07	3.74	3.09	3.14	3.58	**3.04**
	Pr	3.42	3.78	3.13	3.18	3.62	**3.08**
	Nd	3.27	3.83	3.18	3.23	3.67	**3.13**
	Sm	**2.74**	3.71	3.06	3.11	3.55	3.01
	Eu	**2.71**	3.94	3.29	3.34	3.78	3.24
	Gd	**2.50**	3.91	3.26	3.31	3.75	3.21
	Tb	**2.32**	3.83	3.18	3.23	3.67	3.13
	Dy	**2.24**	3.98	3.33	3.38	3.82	3.28
	Ho	**2.46**	4.05	3.40	3.45	3.89	3.35
	Er	**2.12**	4.01	3.36	3.41	3.85	3.31
	Tm	**1.92**	4.08	3.43	3.48	3.92	3.38
	Yb	**2.18**	4.10	3.45	3.50	3.94	3.40
	Lu	**1.85**	4.21	3.56	3.61	4.05	3.51

and thus the formation energy of any defect involving F^- interstitials, should be larger in $LiCaAlF_6$ than in $LiSrAlF_6$. Again, the values in table 3 indicate that this difference is about 6%, enough to make the formation energy of the LiF pseudo anti-Schottky defect greater than that for the Li^+ Frenkel pair in the $LiCaAlF_6$system.

5.2. Rare earth doping

Predictions of the sites occupied by rare earth dopants are made using the calculated solution energies. It is clear that defect–defect interactions play an important role in lowering these energies, so the bound solution energies reported in tables 8(a), (b) and 10 are used. In the following discussion of trends, $LiCaAlF_6$ and $LiSrAlF_6$ are considered separately. Use is made of the numbering of solution energy schemes given in section 4.2.

Table 8. Solution energies (in eV) for rare earth dopants (M) in (a) $LiCaAlF_6$ at Al^{3+} and Ca^{2+} sites (b) $LiSrAlF_6$ at Al^{3+} and Sr^{2+} sites (schemes (i)–(iv) in table 5) assuming the defects to be bound. Lowest energy solution schemes are highlighted in bold; where no value is highlighted, see table 10 for the favoured scheme. nc denotes non-convergence.

(a)		$M^{\bullet}_{Ca}-\frac{1}{2}V''_{Ca}$			$M^{\bullet}_{Ca}-F_i'$		
Scheme from table 5	M_{Al} (i)	(ii) RE at ($\pm$100)	(ii) RE at (00 ± 1)	$M^{\bullet}_{Ca}-V'_{Li}$ (iii)	(iv) F_i' at ($\frac{1}{4}\ \frac{1}{4}\ 0$)	(iv) F_i' at ($\frac{1}{2}\ \frac{1}{2}\ 0$)	(iv) F_i' at ($\frac{3}{4}\ \frac{1}{2}\ 0$)
La	4.20	2.39	2.35	**1.89**	1.99	2.13	2.17
Ce	3.96	2.41	2.35	1.89	1.97	2.11	2.15
Pr	3.72	2.42	2.34	**1.89**	1.96	2.09	2.30
Nd	3.56	2.44	2.35	**1.90**	1.95	2.08	2.59
Sm	3.00	2.31	2.23	**1.75**	6.45	1.95	1.98
Eu	2.95	2.50	2.40	**1.92**	2.59	2.09	2.11
Gd	2.72	2.46	2.37	**1.87**	1.94	1.06	1.95
Tb	2.54	2.38	2.30	**1.79**	2.26	1.99	1.91
Dy	2.44	2.51	2.42	**1.90**	nc	2.09	2.10
Ho	2.67	2.57	2.43	**1.96**	1.98	2.10	2.10
Er	2.32	2.51	2.40	**1.89**	1.94	2.07	1.99
Tm	2.10	2.58	2.49	**1.95**	2.43	2.17	2.14
Yb	2.37	2.59	2.46	**1.97**	2.11	2.12	2.10
Lu	**2.01**	2.68	2.60	2.05	2.53	2.27	2.15
(b)		$M^{\bullet}_{Sr}-\frac{1}{2}V''_{Sr}$			$M^{\bullet}_{Sr}-F_i'$		
Scheme from table 5	M_{Al} (i)	(ii) RE at ($\pm$100)	(ii) RE at (00 ± 1)	$M^{\bullet}_{Sr}-V'_{Li}$ (iii)	(iv) F_i' at ($\frac{1}{4}\ \frac{1}{4}\ 0$)	(iv) F_i' at ($\frac{1}{2}\ \frac{1}{2}\ 0$)	(iv) F_i' at ($\frac{3}{4}\ \frac{1}{2}\ 0$)
La	3.86	2.75	2.82	2.29	**1.94**	1.94	1.96
Ce	3.64	2.81	2.88	2.34	1.99	**1.96**	1.99
Pr	3.42	2.86	2.92	2.40	3.66	2.24	**2.01**
Nd	3.27	2.92	2.97	2.46	2.28	5.45	**2.01**
Sm	2.74	2.85	2.87	2.37	**1.92**	**1.92**	**1.92**
Eu	2.71	3.10	3.11	2.59	2.39	**2.12**	2.13
Gd	2.50	3.09	3.08	2.59	6.45	2.38	**2.11**
Tb	2.32	3.02	3.01	2.51	3.41	**2.04**	**2.04**
Dy	2.24	3.19	3.16	2.68	2.74	2.46	**2.19**
Ho	2.46	3.23	3.23	2.74	2.21	**1.99**	2.21
Er	**2.12**	3.22	3.19	2.71	3.14	2.20	2.20
Tm	**1.92**	3.32	3.27	2.79	2.54	2.58	2.31
Yb	**2.18**	3.31	3.29	2.80	2.89	2.55	2.27
Lu	**1.85**	3.46	3.41	2.92	2.44	2.44	2.45

Considering $LiCaAlF_6$ (tables 8(a) and 10), for La, scheme (iii) is preferred (substitution at the Ca^{2+} site with Li^+ vacancy compensation), while for Ce, scheme (vi) is favoured (substitution at the Li^+ site with Ca^{2+} vacancy compensation). For the series from Pr–Tm, these two schemes give very similar energies, although exceptions include Sm, which prefers scheme (iii), and Gd, for which scheme (iv) (substitution at the Ca^{2+} site with F^- interstitial compensation) is preferred. For Yb, scheme (iii) is preferred, while for Lu, there is a small energetic preference for scheme (i), with scheme (iii) coming second. However, it is noted that in most cases, scheme (iv) is either the second or third most favourable scheme.

Table 9. Solution energies (in eV) for rare earth dopants (M) in (a) $LiCaAlF_6$ at Li^+ sites (b) $LiSrAlF_6$ at Li^+ sites (schemes (v)–(vii) in table 5) assuming the defects to be unbound. Lowest energies are highlighted in bold.

(a) Scheme from table 5	$M^{\bullet\bullet}_{Li}$–$2V'_{Li}$ (v)	$M^{\bullet\bullet}_{Li}$–V''_{Ca} (vi)	$M^{\bullet\bullet}_{Li}$–$2F_i'$ (vii) F_i' at $(\frac{1}{4}\ \frac{1}{4}\ 0)$	$M^{\bullet\bullet}_{Li}$–$2F_i'$ (vii) F_i' at $(\frac{1}{2}\ \frac{1}{2}\ 0)$	$M^{\bullet\bullet}_{Li}$–$2F_i'$ (vii) F_i' at $(\frac{3}{4}\ \frac{1}{2}\ 0)$
La	11.49	**11.30**	12.71	13.07	13.07
Ce	11.30	**11.11**	12.52	12.88	12.88
Pr	11.07	**10.88**	11.99	12.65	12.65
Nd	10.96	**10.77**	12.18	12.54	12.54
Sm	10.51	**10.32**	11.73	12.09	12.09
Eu	10.48	**10.29**	11.70	12.06	12.06
Gd	10.31	**10.12**	11.53	11.89	11.89
Tb	10.15	**9.96**	11.37	11.73	11.73
Dy	10.09	**9.90**	11.31	11.67	11.67
Ho	10.23	**10.04**	11.45	11.81	11.81
Er	9.97	**9.78**	11.19	11.55	11.55
Tm	9.83	**9.64**	11.05	11.41	11.41
Yb	10.3	**9.81**	11.22	11.58	11.58
Lu	9.77	**9.58**	10.99	11.35	11.35

(b) Scheme from table 5	$M^{\bullet\bullet}_{Li}$–$2V'_{Li}$ (v)	$M^{\bullet\bullet}_{Li}$–V''_{Sr} (vi)	$M^{\bullet\bullet}_{Li}$–$2F_i'$ (vii) F_i' at $(\frac{1}{4}\ \frac{1}{4}\ 0)$	$M^{\bullet\bullet}_{Li}$–$2F_i'$ (vii) F_i' at $(\frac{1}{2}\ \frac{1}{2}\ 0)$	$M^{\bullet\bullet}_{Li}$–$2F_i'$ (vii) F_i' at $(\frac{3}{4}\ \frac{1}{2}\ 0)$
La	**9.41**	10.70	9.51	10.39	9.31
Ce	**9.22**	10.51	9.32	10.20	9.12
Pr	**9.04**	10.33	9.14	10.02	8.94
Nd	**9.48**	10.21	9.58	9.90	9.38
Sm	**8.47**	9.76	8.57	9.45	8.37
Eu	**8.46**	9.75	8.56	9.44	8.36
Gd	**8.19**	9.58	8.29	9.27	8.09
Tb	**8.13**	9.42	8.23	9.11	8.03
Dy	**8.08**	9.37	8.18	9.06	7.98
Ho	**8.24**	9.53	8.34	9.22	8.14
Er	**7.98**	9.27	8.08	8.96	7.88
Tm	**7.84**	9.13	7.94	8.82	7.74
Yb	**8.02**	9.31	8.12	9.00	7.92
Lu	**7.79**	9.08	7.89	8.77	7.69

For $LiSrAlF_6$ (tables 8(b) and 10) the rare earth series is found to split into two sections. From La–Ho, scheme (iv) (substitution at the Sr^{2+} site with F^- interstitial compensation) is favoured, and from Er–Lu, scheme (i) (substitution at the Al^{3+} site) is preferred.

The different behaviour of the two materials may be rationalized as follows. For $LiCaAlF_6$, the lattice parameters are smaller than those in $LiSrAlF_6$, and it is for this reason that charge compensation by vacancies is favoured over interstitials in almost all cases. For the same reason the Al^{3+} site cannot accommodate most of the rare earth ions, apart from the very smallest one, Lu. In contrast, although the Al^{3+} site is about the same size in both matrices (Al–F distance $\sim$1.80 Å [9, 10]), the larger lattice parameter in $LiSrAlF_6$ allows outward relaxation of the 6 F^- ions surrounding the Al^{3+} site to accommodate the rare earth ions, and this is reflected in the fact that more of the rare earth series can be accommodated here. Similarly there is more room in the lattice for interstitial defects, which explains why the preferred charge compensation scheme for the larger rare earth ions involves F^- interstitials.

Table 10. Solution energies (in eV) for rare earth dopants substituting at Li^+ sites in $LiCaAlF_6$ and $LiSrAlF_6$ (scheme (vi) in table 5), assuming the defects to be bound. Lowest energy solution schemes are highlighted in bold; where no value is highlighted, see table 8(a) or (b) for the favoured scheme. nc denotes non-convergence.

Scheme from table 5	$M_{Li}^{\bullet\bullet}$–V''_{Ca} (vi) $LiCaAlF_6$	$M_{Li}^{\bullet\bullet}$–V''_{Sr} (vi) $LiSrAlF_6$
La	1.99	nc
Ce	**1.45**	2.36
Pr	**1.89**	nc
Nd	**1.90**	2.48
Sm	6.10	2.39
Eu	**1.92**	5.29
Gd	**1.88**	2.61
Tb	**1.80**	2.54
Dy	**1.90**	5.19
Ho	**1.96**	nc
Er	**1.90**	5.19
Tm	**1.95**	5.38
Yb	5.25	nc
Lu	nc	5.59

The reason for including the unbound solution energies is to emphasize the importance of binding energies in the stabilization of doped ions, which can be as much as ∼2 eV in some cases. This energy contribution is often enough to change the prediction of the lowest energy site. For example, in the case of $LiSrAlF_6$, comparing tables 7(b) and 8(b), it can be seen that in the case of the unbound defects, from Sm onwards there is a clear preference for substitution at the Al^{3+} site, whereas in the bound case substitution at the Sr^{2+} site with F^- interstitial compensation becomes more favourable. Since the binding has the effect of lowering the solution energies, it can be predicted that in a real system the defects would also be bound. This will certainly affect the transport properties of the materials, and the effect can be detected by a range of experimental techniques. It may also affect the laser activity of the materials, since the presence of the charge-compensating defect close to the active centre can quench the luminescence and therefore decrease the efficiency of the laser. For this reason, the most efficient combinations of dopants and host would be the ones involving substitution at the Al^{3+} site, e.g. Lu in both hosts, and Dy, Er, Tm and Yb in $LiSrAlF_6$.

6. Conclusions

The paper has presented a detailed study of defect structure and rare earth doping in $LiCaAlF_6$ and $LiSrAlF_6$. The preferred sites for doping have been calculated and rationalized on the basis of the structural differences between the two materials. Predictions have been made of the most efficient dopant–host combinations for solid-state laser applications.

Acknowledgments

The authors are grateful to CNPq and CAPES for financial support. JBA acknowledges the award of a studentship grant from PIBIC/CNPq-UFS, and DFP thanks Keele University for payment of tuition fees for the MPhil programme.

References

[1] Hughes D W and Barr J R M 1992 *J. Phys. D: Appl. Phys.* **25** 563
[2] Sarantopolou E, Kollia Z and Cefalas A C 2000 *Microelectron. Eng.* **53** 105
[3] Liu Z, Kozeki T, Suzuki Y and Sarukura N 2001 *Opt. Lett.* **26** 301
[4] Dubinskii M A, Semashko V V, Naumov A K, Abdulsabirov R Y and Korableva S L 1993 *Laser Phys.* **3** 216
[5] Marshall C D, Payne S A, Speth J A, Krupke W F, Quarles G J, Castillo V and Chai B H T 1994 *J. Opt. Soc. Am.* B **11** 2054
[6] Jackson R A, Valerio M E G and de Lima J F 2001 *J. Phys.: Condens. Matter* **13** 2147
[7] Mott N F and Littleton M J 1938 *Trans. Faraday Soc.* **34** 485
[8] Valerio M E G, Jackson R A and de Lima J F 2000 *J. Phys.: Condens. Matter* **12** 7727
[9] Bolotina N B, Maximov B A, Simonov V I, Derzhavin S I, Uvarova T V and Apollonov V V 1993 *Kristallografiya (Crystal. Rep.)* **38** 43
[10] Schaffers K I and Keszler D A 1991 *Acta Crystallogr.* C **47** 18
[11] Jackson R A, Valerio M E G and de Lima J F 1996 *J. Phys.: Condens. Matter* **8** 10931
[12] Valerio M E G, Jackson R A and de Lima J F 1998 *J. Phys.: Condens. Matter* **10** 3353
[13] Binks D J 1994 *PhD Thesis* University of Surrey, UK
[14] Chadwick A V 1994 *Encyclopaedia of Applied Physics* vol 8 (New York: VCH) p 193